

# Compact implementation of the (SWAP)<sup>a</sup> gate on diamond nitrogen-vacancy centers coupled to resonators

Hai-Rui Wei · Fu-Guo Deng

Received: 10 January 2014 / Accepted: 23 October 2014 / Published online: 4 November 2014  
© Springer Science+Business Media New York 2014

**Abstract** A compact quantum circuit for implementing the (SWAP)<sup>a</sup> gate for  $0 < a \leq 1$  on two diamond nitrogen-vacancy centers (NV) is designed by using some input–output processes of a single photon. Our proposal is interesting because the (SWAP)<sup>a</sup> gate is universal for quantum computing, and the diamond NV center has a long coherence time. Our scheme is compact, and additional electronic qubits are not employed, which beats its synthesis procedure in terms of controlled-not gates and single-qubit rotations largely. Moreover, our scheme is feasible with current experiment technology.

**Keywords** Quantum computing · Quantum logic gate · Diamond nitrogen-vacancy center · Quantum electrodynamics

## 1 Introduction

Quantum logic gates are important in quantum computation because they are the essential building blocks in a quantum computer [1]. The quantum circuits should be optimized with respect to the number of the elementary quantum gates. One of the most efficient quantum gate is the (SWAP)<sup>a</sup> gate for  $0 < a \leq 1$  [2–4] and it is equally efficient as the controlled-not (CNOT) gate in two-qubit quantum computation. The (SWAP)<sup>a</sup> gate provides a different way to implement quantum computing without CNOT gates, and 3 (SWAP)<sup>a</sup> gates combined with 6 single-qubit gates can realize an arbitrary two-qubit unitary operation [2]. A square-root-of-SWAP ( $\sqrt{\text{SWAP}}$ ) gate is a only maximal entangler in the (SWAP)<sup>a</sup> family [4], and  $\{\sqrt{\text{SWAP}}\}$  gates, arbitrary

---

H.-R. Wei · F.-G. Deng (✉)  
Department of Physics, Applied Optics Beijing Area Major Laboratory, Beijing Normal University,  
Beijing 100875, China  
e-mail: fgdeng@bnu.edu.cn

single-qubit rotations} is a universal set of quantum gates [5]. The SWAP gate itself is not universal. However, it is widely used in quantum computation and quantum information processing. It can be used to construct optimal quantum circuits, store quantum information, and teleport the quantum state. Therefore, the project for implementing a (SWAP)<sup>a</sup> gate is highly desired for quantum computing.

Many studies were focused on physically implementing universal quantum gates [6–28], and the ones acting on solid-state qubits have been identified as the prominent candidates for a scalable quantum computer because of their long coherence times and their good scalability. A single diamond nitrogen-vacancy (NV) defect center is regarded as the most exceptional matter qubit involved in the gate due to its ultralong coherence times, even at the room temperature [29]. Active quantum control on diamond NV centers (such as initialization [30], single-qubit manipulation [31,32], and measurement [33]), crucial for quantum information processing, has been achieved by using well-developed techniques. Based on diamond NV centers, people proposed some interesting schemes for universal quantum computing on electron-spin qubits [34–36], hybrid electron-nuclear spin qubits [37,38], or photonic polarization qubits [39], and hyperentanglement purification and concentration [40]. The light-matter system coupled to a cavity, preserving the advantages of the photon and the matter, served as a platform for quantum information processing [10,41–50].

In this paper, we investigate the implementation of the (SWAP)<sup>a</sup> gate on two electron-spin qubits associated with the diamond NV centers, achieved by some input–output processes of a single photon. The qubits involved in this gate encoded in the two electronic ground triple states of the NV centers, i.e.,  $|m_s = +1\rangle$  and  $|m_s = -1\rangle$ , and they have a long decoherence time even at the room temperature. Two well designed quantum circuits are proposed by interacting a single photon with the NV centers and some feed-forward classical operations. The single-qubit gates can be achieved by microwave. An advantage of our schemes is that our quantum circuits are compact and simple, and they do not resort to additional electron-spin qubits. The complexity of our schemes beats their optimal synthesis largely. The evaluation of the fidelity and efficiency of the gate shows that our schemes are feasible in experiment.

## 2 Compact quantum circuit for implementing (SWAP)<sup>a</sup> gate

Let us consider two separate negatively diamond NV centers and each NV center is confined in a resonator, shown in Fig. 1. The cavity supports two polarization-degenerate photons, the left-circularly polarized photon  $|L\rangle$  and the right-circularly polarized photon  $|R\rangle$ . The unpolarized cavities can be achieved by using H1 photonic crystal [51], micropillars [52–54], or fiber-based ones [55]. In the absence of a magnetic field, the electronic ground spin triple states of each NV center have a 2.88 GHz splitting between the sublevels  $|0\rangle = |m_s = 0\rangle$  and  $|\pm\rangle = |m_s = \pm 1\rangle$  owing to the spin–spin interaction [56]. The degeneracy between  $|+\rangle$  and  $|-\rangle$  is lifted by an external static magnetic field. One of the six excited states [57]  $|A_2\rangle = (|E_-\rangle|+\rangle + |E_+\rangle|-\rangle)/\sqrt{2}$  is employed as an ancillary level.  $|A_2\rangle$  is robust against low strain and magnetic field. The spin-selective optical transitions  $|\pm\rangle \rightarrow |A_2\rangle$  are assisted by the

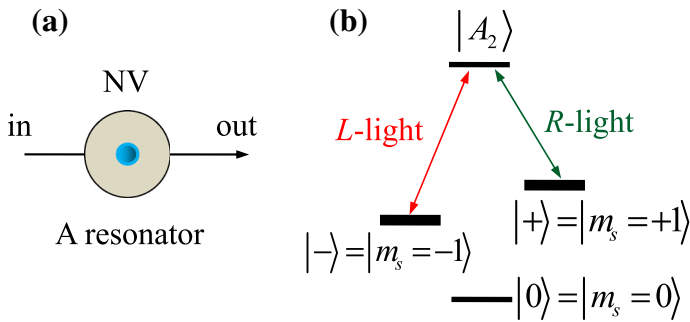


**Fig. 1** **a** Schematic diagram of a diamond NV center confined in a resonator. **b** The  $\Lambda$ -type level configuration of the diamond NV center.  $R$  and  $L$  present the *right*-circularly polarized and the *left*-circularly polarized photons, respectively.  $|A_2\rangle = (|E_-\rangle|+\rangle + |E_+\rangle|-\rangle)/\sqrt{2}$  is the ancillary level

$R$ -polarized and  $L$ -polarized photons, respectively.  $|E_{\pm}\rangle$  are the orbital states with the angular momentum projections  $\pm 1$  along the NV axis.

The Heisenberg equations of the motion for the cavity mode  $\hat{a}$  driven by the input field  $\hat{a}_{in}(t)$  with the frequency  $\omega_c$ , the NV lowering operator  $\sigma_-$  with the frequency  $\omega_0$ , and the input–output relation for the cavity are [58]

$$\begin{aligned} \dot{\hat{a}} &= [i(\omega_c - \omega_p) + \kappa/2] \hat{a}(t) - g\sigma_-(t) - \sqrt{\kappa} \hat{a}_{in}, \\ \dot{\sigma}_- &= -[i(\omega_0 - \omega_p) + \gamma/2] \sigma_-(t) - g\sigma_z(t) \hat{a}(t) + \sqrt{\gamma} \sigma_z(t) \hat{b}_{in}(t), \\ \hat{a}_{out} &= \hat{a}_{in} + \sqrt{\kappa} \hat{a}(t). \end{aligned} \tag{1}$$

With a weak excitation  $\langle \sigma_z \rangle = -1$ , Chen et al. [59,60] obtained the reflection coefficient of the NV center inside a single-side cavity unit as

$$r(\omega_p) = \frac{[i(\omega_c - \omega_p) - \frac{\kappa}{2}][i(\omega_0 - \omega_p) + \frac{\gamma}{2}] + g^2}{[i(\omega_c - \omega_p) + \frac{\kappa}{2}][i(\omega_0 - \omega_p) + \frac{\gamma}{2}] + g^2}. \tag{2}$$

Here,  $\omega_p$  is the frequency of the incident photon.  $\sigma_z(t)$  is the inversion operator of the NV center.  $\kappa$  and  $\gamma$  are the decay rates of the cavity and the NV center, respectively.  $g$  is the coupling strength between the cavity and the NV center.  $b_{in}(t)$  is the vacuum input field felt by the NV center with the commutation relation  $[\hat{b}_{in}(t), \hat{b}_{in}^\dagger(t')] = \delta(t - t')$ .

In the present study, we consider the transition  $|-\rangle \rightarrow |A_2\rangle$  matches the  $L$ -polarized component of the input single photon under the resonant condition  $\omega_c = \omega_0 = \omega_p$ . If the NV center is in the state  $|-\rangle$ , the  $L$ -polarized photon senses the hot cavity, i.e.,  $g \neq 0$  and acquires a phase shift of  $\varphi$ , while the  $R$ -polarized photon senses the cold cavity, i.e.,  $g = 0$  due to the polarization mismatch and acquires a phase shift of  $\varphi_0$ . As a result,  $|L\rangle|-\rangle \xrightarrow{\text{cav}} e^{i\varphi}|r||L\rangle|-\rangle$  and  $|R\rangle|-\rangle \xrightarrow{\text{cav}} e^{i\varphi_0}|r_0||R\rangle|-\rangle$ .  $r_0$  is given by Eq. (2) with  $g = 0$ . In the case that the NV center is in the state  $|+\rangle$ , both  $R$ -polarized and  $L$ -polarized photons sense the cold cavity due to the large detuning and they acquire a phase shift of  $\varphi_0$ . Therefore,  $|L\rangle|+\rangle \xrightarrow{\text{cav}} e^{i\varphi_0}|r_0||L\rangle|+\rangle$  and  $|R\rangle|+\rangle \xrightarrow{\text{cav}} e^{i\varphi_0}|r_0||R\rangle|+\rangle$ .

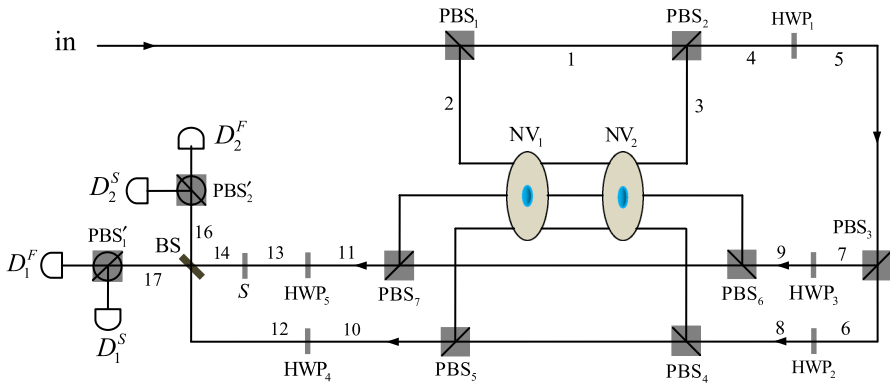


**Fig. 2** Compact quantum circuit for implementing the  $(\text{SWAP})^a$  gate on two diamond NV centers. BS is a 50:50 beam splitter.  $S = e^{i\pi a}|R\rangle\langle R| + |L\rangle\langle L|$  is a one-qubit phase gate.  $\text{PBS}_j (j = 1, 2, \dots)$  presents a polarizing beam splitter in the circularly polarized basis  $\{|R\rangle, |L\rangle\}$ , which transmits the  $R$ -polarized photons and reflects the  $L$ -polarized photons.  $\text{PBS}'_j$  presents a PBS which is rotated  $+45^\circ$  with respect to the  $\{|R\rangle, |L\rangle\}$  basis.  $\text{HWP}_j$  is a half-wave plate.  $D_j^F$  and  $D_j^S$  are two single-photon detectors

Chen et al. [60] showed that  $r(\omega_p) \simeq 1$  and  $r_0(\omega_p) = -1$  when  $g \geq 5\sqrt{\gamma\kappa}$  and  $\omega_c = \omega_0 = \omega_p$ . The changes of the input photon can be summarized as

$$\begin{aligned} |R\rangle|-\rangle &\rightarrow -|R\rangle|-\rangle, & |L\rangle|-\rangle &\rightarrow |L\rangle|-\rangle, & |R\rangle|+\rangle &\rightarrow -|R\rangle|+\rangle, \\ |L\rangle|+\rangle &\rightarrow -|L\rangle|+\rangle. \end{aligned} \tag{3}$$

The matrix representation of the  $(\text{SWAP})^a$  gate acting on two NV centers is given by

$$U_{(\text{SWAP})^a} = \begin{pmatrix} 1 & 0 & 0 & 0 \\ 0 & \frac{1+e^{i\pi a}}{2} & \frac{1-e^{i\pi a}}{2} & 0 \\ 0 & \frac{1-e^{i\pi a}}{2} & \frac{1+e^{i\pi a}}{2} & 0 \\ 0 & 0 & 0 & 1 \end{pmatrix} \tag{4}$$

in the basis  $\{|+\rangle_1|+\rangle_2, |+\rangle_1|-\rangle_2, |-\rangle_1|+\rangle_2, |-\rangle_1|-\rangle_2\}$ . The schematic diagram for implementing the  $(\text{SWAP})^a$  gate acting on two NV centers is shown in Fig. 2. Suppose the system composed of the two NV centers  $\text{NV}_1$  and  $\text{NV}_2$  is initially prepared in the state

$$|\Phi\rangle^e = (\cos \alpha|+\rangle_1 + \sin \alpha|-\rangle_1) \otimes (\cos \beta|+\rangle_2 + \sin \beta|-\rangle_2). \tag{5}$$

The single-photon medium is initially prepared in an equal superposition of  $|R\rangle$  and  $|L\rangle$ , i.e.,

$$|\Phi\rangle^p = \frac{1}{\sqrt{2}}(|R\rangle + |L\rangle). \tag{6}$$

From the function of the (SWAP)<sup>a</sup> gate described by Eq. (4), one can see that the key ingredient of the protocol for implementing such a gate is to accomplish the following transformations

$$\begin{aligned}
 |+\rangle_1|+\rangle_2 &\rightarrow \frac{1}{2}(|+\rangle_1|+\rangle_2 + |+\rangle_1|-\rangle_2 + |-\rangle_1|+\rangle_2 + |-\rangle_1|-\rangle_2) \xrightarrow{H^{e_1 \otimes e_2}} |+\rangle_1|+\rangle_2, \\
 |+\rangle_1|-\rangle_2 &\rightarrow \frac{1}{2}(|+\rangle_1|+\rangle_2 - e^{i\pi a}|+\rangle_1|-\rangle_2 + e^{i\pi a}|-\rangle_1|+\rangle_2 \\
 &\quad - |-\rangle_1|-\rangle_2) \xrightarrow{H^{e_1 \otimes e_2}} \frac{1 + e^{i\pi a}}{2}|+\rangle_1|-\rangle_2 + \frac{1 - e^{i\pi a}}{2}|-\rangle_1|+\rangle_2, \\
 |-\rangle_1|+\rangle_2 &\rightarrow \frac{1}{2}(|+\rangle_1|+\rangle_2 + e^{i\pi a}|+\rangle_1|-\rangle_2 - e^{i\pi a}|-\rangle_1|+\rangle_2 \\
 &\quad - |-\rangle_1|-\rangle_2) \xrightarrow{H^{e_1 \otimes e_2}} \frac{1 - e^{i\pi a}}{2}|+\rangle_1|-\rangle_2 + \frac{1 + e^{i\pi a}}{2}|-\rangle_1|+\rangle_2, \\
 |-\rangle_1|-\rangle_2 &\rightarrow \frac{1}{2}(|+\rangle_1|+\rangle_2 - |+\rangle_1|-\rangle_2 - |-\rangle_1|+\rangle_2 + |-\rangle_1|-\rangle_2) \xrightarrow{H^{e_1 \otimes e_2}} |-\rangle_1|-\rangle_2.
 \end{aligned}
 \tag{7}$$

The evolution of the states  $|+\rangle_1|+\rangle_2$  and  $|-\rangle_1|-\rangle_2$  is independent of  $|+\rangle_1|-\rangle_2$  and  $|-\rangle_1|+\rangle_2$  can be achieved by the upper part of Fig. 2.  $H^{e_1}$  ( $H^{e_2}$ ) is a Hadamard operation performed on  $NV_1$  ( $NV_2$ ). The action of an  $H^e$  is given by

$$|+\rangle \xrightarrow{H^e} \frac{1}{\sqrt{2}}(|+\rangle + |-\rangle), \quad |-\rangle \xrightarrow{H^e} \frac{1}{\sqrt{2}}(|+\rangle - |-\rangle).
 \tag{8}$$

In the following, let us discuss the construction of the solid-state (SWAP)<sup>a</sup> gate on a two-qubit NV-center system step by step.

First, the single photon is injected into the input port *in*, and then it is split into two parts by the polarizing beam splitter PBS<sub>1</sub>. The *L*-polarized component goes through  $NV_1$  and  $NV_2$  in succession, and then it reaches PBS<sub>2</sub> simultaneously with the *R*-polarized component. Subsequently, the photon goes through the half-wave plate HWP<sub>1</sub> and arrives at PBS<sub>3</sub>. Here, HWP<sub>1</sub> oriented at 22.5° results in a Hadamard operation  $H^P$  on the polarization of the photon

$$|R\rangle \xrightarrow{H^P} |F\rangle \equiv \frac{1}{\sqrt{2}}(|R\rangle + |L\rangle), \quad |L\rangle \xrightarrow{H^P} |S\rangle \equiv \frac{1}{\sqrt{2}}(|R\rangle - |L\rangle).
 \tag{9}$$

The above operations (PBS<sub>1</sub> →  $NV_1, NV_2$  → PBS<sub>2</sub> → HWP<sub>1</sub> → PBS<sub>3</sub>) transform the state of the complicated system composed of the two NV centers and the single photon from  $|\Phi_0\rangle$  to  $|\Phi_1\rangle$ . Here,

$$\begin{aligned}
 |\Phi_0\rangle &= |\Phi\rangle^P \otimes |\Phi\rangle^e, \\
 |\Phi_1\rangle &= \cos \alpha |+\rangle_1 (\cos \beta |R\rangle_6 |+\rangle_2 + \sin \beta |L\rangle_7 |-\rangle_2) + \sin \alpha |-\rangle_1 (\cos \beta |L\rangle_7 |+\rangle_2 \\
 &\quad + \sin \beta |R\rangle_6 |-\rangle_2).
 \end{aligned}
 \tag{10}$$

The block composed of PBS<sub>1</sub>,  $NV_1, NV_2$ , and PBS<sub>2</sub> completes the transformation

$$U_{\text{block}} = \begin{pmatrix} I_5 & 0 & 0 & 0 \\ 0 & -1 & 0 & 0 \\ 0 & 0 & -1 & 0 \\ 0 & 0 & 0 & 1 \end{pmatrix} \tag{11}$$

in the basis  $\{|R\rangle|+\rangle_1|+\rangle_2, |R\rangle|+\rangle_1|-\rangle_2, |R\rangle|-\rangle_1|+\rangle_2, |R\rangle|-\rangle_1|-\rangle_2, |L\rangle|+\rangle_1|+\rangle_2, |L\rangle|+\rangle_1|-\rangle_2, |L\rangle|-\rangle_1|+\rangle_2, |L\rangle|-\rangle_1|-\rangle_2\}$ . Here,  $I_5$  is a  $5 \times 5$  unit matrix.  $|R\rangle_j$  ( $|L\rangle_j$ ) denotes the  $R$ -polarized ( $L$ -polarized) wavepacket emitted from the spatial mode  $j$ .

Second, before and after the photon emitting from the spatial mode 6 (7) interacts with the block composed of PBS<sub>4</sub>, NV<sub>2</sub>, NV<sub>1</sub>, and PBS<sub>5</sub> (PBS<sub>6</sub>, NV<sub>2</sub>, NV<sub>1</sub>, and PBS<sub>7</sub>) described by Eq. (11), an  $H^p$  is performed on the photon with HWP<sub>2</sub> and HWP<sub>4</sub> (HWP<sub>3</sub> and HWP<sub>5</sub>), and an  $H^e$  is performed on each of the two NV centers before the photon goes through the block. When the photon emits from the spatial mode 12, it reaches the 50:50 beam splitter (BS) directly. When the photon emits from the spatial mode 13, before it reaches the BS, a single-qubit phase operation  $S = e^{i\pi a}|R\rangle\langle R| + |L\rangle\langle L|$  is performed on it with a half-wave plate. The above operations (HWP<sub>2</sub>,  $H^{e2 \otimes e1} \rightarrow$  PBS<sub>4</sub>  $\rightarrow$  NV<sub>2</sub>, NV<sub>1</sub>  $\rightarrow$  PBS<sub>5</sub>  $\rightarrow$  HWP<sub>4</sub> and HWP<sub>3</sub>,  $H^{e2 \otimes e1} \rightarrow$  PBS<sub>6</sub>  $\rightarrow$  NV<sub>2</sub>, NV<sub>1</sub>  $\rightarrow$  PBS<sub>7</sub>  $\rightarrow$  HWP<sub>5</sub>  $\rightarrow$  S) transform the state of the complicated system into

$$\begin{aligned} |\Phi\rangle_2 = & \frac{\cos \alpha \cos \beta}{2} [ |R\rangle_{12}|+\rangle_1|+\rangle_2 + |L\rangle_{12}|+\rangle_1|-\rangle_2 + |L\rangle_{12}|-\rangle_1|+\rangle_2 \\ & + |R\rangle_{12}|-\rangle_1|-\rangle_2 ] \\ & + \frac{\cos \alpha \sin \beta}{2} [ |L\rangle_{14}|+\rangle_1|+\rangle_2 - e^{i\pi a}|R\rangle_{14}|+\rangle_1|-\rangle_2 + e^{i\pi a}|R\rangle_{14}|-\rangle_1|+\rangle_2 \\ & - |L\rangle_{14}|-\rangle_1|-\rangle_2 ] \\ & + \frac{\sin \alpha \cos \beta}{2} [ |L\rangle_{14}|+\rangle_1|+\rangle_2 + e^{i\pi a}|R\rangle_{14}|+\rangle_1|-\rangle_2 - e^{i\pi a}|R\rangle_{14}|-\rangle_1|+\rangle_2 \\ & - |L\rangle_{14}|-\rangle_1|-\rangle_2 ] \\ & + \frac{\sin \alpha \sin \beta}{2} [ |R\rangle_{12}|+\rangle_1|+\rangle_2 - |L\rangle_{12}|+\rangle_1|-\rangle_2 - |L\rangle_{12}|-\rangle_1|+\rangle_2 \\ & + |R\rangle_{12}|-\rangle_1|-\rangle_2 ]. \end{aligned} \tag{12}$$

Subsequently, the wavepackets are mixed at the BS, and an  $H^e$  is performed on each of the two NV centers. The state of the complicated system becomes

$$\begin{aligned} |\Phi\rangle_3 = & \frac{|F\rangle_{16}}{2} [ \cos \alpha \cos \beta |+\rangle_1|+\rangle_2 \\ & + \cos \alpha \sin \beta \left( \frac{1 + e^{i\pi a}}{2} |+\rangle_1|-\rangle_2 + \frac{1 - e^{i\pi a}}{2} |-\rangle_1|+\rangle_2 \right) \\ & + \sin \alpha \cos \beta \left( \frac{1 - e^{i\pi a}}{2} |+\rangle_1|-\rangle_2 + \frac{1 + e^{i\pi a}}{2} |-\rangle_1|+\rangle_2 \right) \\ & + \sin \alpha \sin \beta |-\rangle_1|-\rangle_2 ] \end{aligned}$$

$$\begin{aligned}
 & + \frac{|S\rangle_{16}}{2} \left[ \cos \alpha \cos \beta |-\rangle_1 |-\rangle_2 \right. \\
 & - \cos \alpha \sin \beta \left( \frac{1 - e^{i\pi a}}{2} |+\rangle_1 |-\rangle_2 + \frac{1 + e^{i\pi a}}{2} |-\rangle_1 |+\rangle_2 \right) \\
 & - \sin \alpha \cos \beta \left( \frac{1 + e^{i\pi a}}{2} |+\rangle_1 |-\rangle_2 + \frac{1 - e^{i\pi a}}{2} |-\rangle_1 |+\rangle_2 \right) \\
 & \left. + \sin \alpha \sin \beta |+\rangle_1 |+\rangle_2 \right] \\
 & - \frac{|F\rangle_{17}}{2} \left[ \cos \alpha \cos \beta |+\rangle_1 |+\rangle_2 \right. \\
 & - \cos \alpha \sin \beta \left( \frac{1 + e^{i\pi a}}{2} |+\rangle_1 |-\rangle_2 + \frac{1 - e^{i\pi a}}{2} |-\rangle_1 |+\rangle_2 \right) \\
 & - \sin \alpha \cos \beta \left( \frac{1 - e^{i\pi a}}{2} |+\rangle_1 |-\rangle_2 + \frac{1 + e^{i\pi a}}{2} |-\rangle_1 |+\rangle_2 \right) \\
 & \left. + \sin \alpha \sin \beta |-\rangle_1 |-\rangle_2 \right] \\
 & - \frac{|S\rangle_{17}}{2} \left[ \cos \alpha \cos \beta |-\rangle_1 |-\rangle_2 \right. \\
 & + \cos \alpha \sin \beta \left( \frac{1 - e^{i\pi a}}{2} |+\rangle_1 |-\rangle_2 + \frac{1 + e^{i\pi a}}{2} |-\rangle_1 |+\rangle_2 \right) \\
 & + \sin \alpha \cos \beta \left( \frac{1 + e^{i\pi a}}{2} |+\rangle_1 |-\rangle_2 + \frac{1 - e^{i\pi a}}{2} |-\rangle_1 |+\rangle_2 \right) \\
 & \left. + \sin \alpha \sin \beta |+\rangle_1 |+\rangle_2 \right]. \tag{13}
 \end{aligned}$$

Here, the BS implements the transformations

$$\begin{aligned}
 |R\rangle_{14} & \xrightarrow{\text{BS}} \frac{|R\rangle_{16} + |R\rangle_{17}}{\sqrt{2}}, & |L\rangle_{14} & \xrightarrow{\text{BS}} \frac{|L\rangle_{16} + |L\rangle_{17}}{\sqrt{2}}, & |R\rangle_{12} & \xrightarrow{\text{BS}} \frac{|R\rangle_{16} - |R\rangle_{17}}{\sqrt{2}}, \\
 |L\rangle_{12} & \xrightarrow{\text{BS}} \frac{|L\rangle_{16} - |L\rangle_{17}}{\sqrt{2}}. \tag{14}
 \end{aligned}$$

Third, we measure the output photon in the basis  $\{|F\rangle, |S\rangle\}$  with the detectors  $D_i^F$  and  $D_j^S$ . If the detector  $D_2^F, D_2^S, D_1^F$ , or  $D_1^S$  is clicked,  $I_2, \sigma_z \sigma_x, \sigma_z$ , or  $\sigma_x$  is performed on each of the two NV centers, respectively. Here,  $I_2 = |+\rangle\langle +| + |-\rangle\langle -|$  means doing nothing on an NV center.  $\sigma_z = |+\rangle\langle +| - |-\rangle\langle -|$  and  $\sigma_x = |+\rangle\langle -| + |-\rangle\langle +|$ . After these classical feed-forward operations, the state of the system composed of the two NV centers becomes

$$\begin{aligned}
 |\Phi\rangle_{(\text{SWAP})^a} & = \cos \alpha \cos \beta |+\rangle_1 |+\rangle_2 \\
 & + \cos \alpha \sin \beta \left( \frac{1 + e^{i\pi a}}{2} |+\rangle_1 |-\rangle_2 + \frac{1 - e^{i\pi a}}{2} |-\rangle_1 |+\rangle_2 \right) \\
 & + \sin \alpha \cos \beta \left( \frac{1 - e^{i\pi a}}{2} |+\rangle_1 |-\rangle_2 + \frac{1 + e^{i\pi a}}{2} |-\rangle_1 |+\rangle_2 \right) \\
 & + \sin \alpha \sin \beta |-\rangle_1 |-\rangle_2. \tag{15}
 \end{aligned}$$

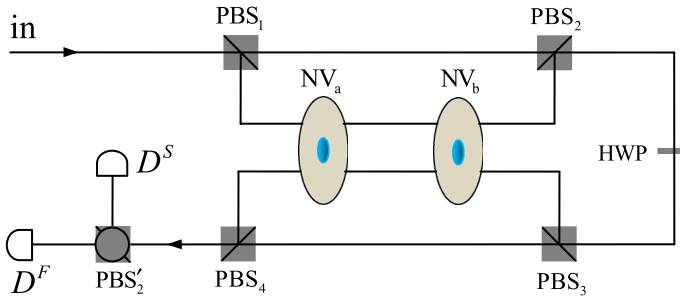


**Fig. 3** Compact quantum circuit for implementing the SWAP gate on two diamond NV centers

From Eq. (15), one can see that the quantum circuit shown in Fig. 2 realizes a more general  $(\text{SWAP})^a$  gate on two NV centers with a success probability of 100% in principle.

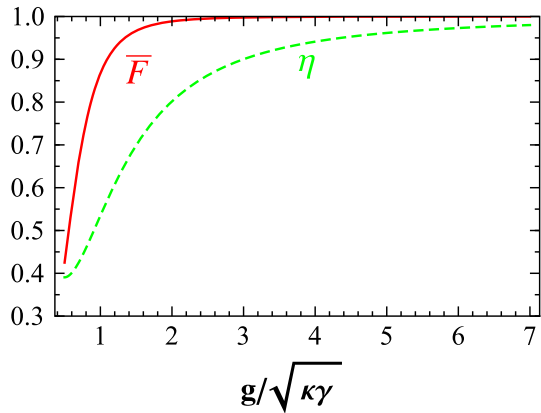
The  $\sqrt{\text{SWAP}}$  gate for  $a = 1/2$  and the SWAP gate for  $a = 1$  can also be implemented with the quantum circuit shown in Fig. 2 with  $S = i|R\rangle\langle R| + |L\rangle\langle L|$  and  $S = -|R\rangle\langle R| + |L\rangle\langle L|$ , respectively. The implementation of a CNOT gate on two NV centers [35] requires a single-photon medium, and two hybrid entangling operations on a photon and an NV center are necessary. According to the synthesis algorithm for finding the optimal quantum circuit in two-qubit operations [61], one can see that the optimal quantum circuit for the  $(\text{SWAP})^a$  gate for  $0 < a \leq 1$  gate requires 3 CNOT gates. Therefore, the quantum circuit for the  $(\text{SWAP})^a$  gate for  $0 < a \leq 1$  shown in Fig. 2 requires less resources than its unstructured synthesis algorithm in Ref. [61] in terms of CNOT gates. The number of the photon medium required 1 beats 3 and the times that the photon passes through the NV centers 4 beats 6. The complexity of the present scheme for a  $\sqrt{\text{SWAP}}$  gate on two NV centers shown in Fig. 2 with  $a = 1/2$  beats its optimal synthesis with CNOT gates as the latter requires at least 3 CNOT gates and 5 single-qubit rotations [62, 63].

The SWAP gate,  $U_{\text{swap}}|\phi\rangle_a \otimes |\phi\rangle_b = |\phi\rangle_b \otimes |\phi\rangle_a$ , exchanges the information of the two qubits. The quantum circuit shown in Fig. 3 can be used to implement the SWAP gate on two NV centers and it is better than its optimal synthesis which requires 3 CNOT gates [1]. The scheme shown in Fig. 3 is also simpler than that shown in Fig. 2.  $H^e$  is performed on each of the two NV centers before and after the photon goes through the block composed of PBS<sub>3</sub>, NV<sub>a</sub>, NV<sub>b</sub>, and PBS<sub>4</sub>. If the detector  $D^F$  is clicked, the gate is achieved; otherwise,  $\sigma_z$  is performed on each of the two NV centers.

So far, the discussion for the construction of the  $(\text{SWAP})^a$  gate on two NV centers is in the case  $g \geq 5\sqrt{\kappa\gamma}$ , i.e.,  $r(\omega_p) \simeq 1$  and  $r_0(\omega_p) = -1$ . Next, we will discuss the influence of  $g/\sqrt{\kappa\gamma}$  on the fidelity and efficiency of the  $(\text{SWAP})^a$  gate. The fidelity of the gate is defined as the overlap of the output states of the system composed of the single photon and the two NV centers in the ideal case  $|\psi_{\text{ideal}}\rangle$  and the real case  $|\psi_{\text{real}}\rangle$ , i.e.,  $F = |\langle\psi_{\text{real}}|\psi_{\text{ideal}}\rangle|^2$ . From above discussion, one can see that in the real case, the spin-selective optical transition rules can be written as



**Fig. 4** The average fidelity (the solid line) and efficiency (the dashed line) of the (SWAP)<sup>a</sup> gate vs the ratio of  $g/\sqrt{\kappa\gamma}$  in the case of  $g/\sqrt{\kappa\gamma} \geq 0.5$



$$|R\rangle|\pm\rangle \rightarrow -|R\rangle|\pm\rangle, \quad |L\rangle|+\rangle \rightarrow -|L\rangle|+\rangle, \quad |L\rangle|-\rangle \rightarrow \frac{4g^2 - \kappa\gamma}{4g^2 + \kappa\gamma}|L\rangle|-\rangle. \tag{16}$$

In this study, we use the average fidelity of the gate defined as  $\bar{F}_{(\text{SWAP})^a} = \frac{1}{4\pi^2} \int_0^{2\pi} d\alpha \int_0^{2\pi} d\beta |\langle \Phi_{\text{real}} | \Phi_{\text{ideal}} \rangle|^2$  to characterize the performance of our (SWAP)<sup>a</sup> gate. Here  $|\Phi_{\text{ideal}}\rangle$  can be described by Eq. (13), and the corresponding output state  $|\Phi_{\text{real}}\rangle$  can be obtain by substituting Eq. (16) for Eq. (3) during the evolution of the whole system. The average fidelity of a family of our (SWAP)<sup>a</sup> gate is independent of  $a$  because the parameter  $a$  is introduced by the single-qubit phase gate  $S$  which is performed after the nonlinear interactions between the photon and the NV centers. The efficiency of the gate is the yield of the photon,  $\eta = n_{\text{output}}/n_{\text{input}}$ , i.e., the number of the output photons  $n_{\text{output}}$  to the input photons  $n_{\text{input}}$ . The efficiency of the (SWAP)<sup>a</sup> gate can be written as

$$\eta = \frac{[4 + (1 + |r|^2)^2]^2}{64}. \tag{17}$$

Manson et al. [56] and Togan et al. [57] showed that the decay rate of the NV center  $\gamma$  within the narrow-band zero phonon line is 3–4% of the NV center’s total decay rate  $\gamma_{\text{tot}} \approx 2\pi \times 15\text{MHz}$ . If the NV center is coupled to a whispering gallery mode resonator [64,65], the coupling strength  $g/2\pi$  can reach 0.3–1GHz and the quantify factor  $Q = c/\lambda\kappa$ . Here,  $c$  is the speed of the light and  $\lambda = 637\text{nm}$ . The experiment showed that a photonic crystal cavity with a quality factor  $Q > 1.5 \times 10^6$  coupled to a diamond NV center can reach the strong coupling regimes  $[g, \kappa, \gamma_{\text{tot}}]/2\pi = [2.25, 0.16, 0.013]\text{GHz}$  [66]. Barclay et al. [64] has demonstrated that the GaP microdisk coupled to an NV center with  $Q \sim 10^4$  can reach the parameters  $[g, \kappa, \gamma_{\text{tot}}, \gamma]/2\pi = [0.3, 26, 0.013, 0.004]\text{GHz}$ .

The average fidelity and efficiency of the (SWAP)<sup>a</sup> gate vary with the ratio of  $g/\sqrt{\kappa\gamma}$ , shown in Fig. 4 in the case of  $g/\sqrt{\kappa\gamma} \geq 0.5$ . From this figure, one can see that our scheme for implementing the (SWAP)<sup>a</sup> gate can reach a high fidelity

and a high efficiency.  $F = 0.999691$  with  $\eta = 0.9615$  when  $g/\sqrt{\kappa\gamma} = 5.0$ .  $F = 0.866944$  with  $\eta = 0.5347$  when  $g/\sqrt{\kappa\gamma} = 1.0$ . In our scheme, the transmitted distance of the single photon is not long, and the operations of the linear optical elements, such as fiber, BS, and HWP are perfect. If the photon is infected by the bit-flip or phase-flip noises during the transmission, the gates we constructed are generally locally equivalent to the  $(\text{SWAP})^a$  or SWAP gates. We can use the success instances in the postselection in the applications to successfully herald our schemes. Charge fluctuations near the NV center and the imperfect electron-spin initiation reduce the fidelities of our schemes [67]. The influence by these two factors can be decreased by independently resetting the charge and resonance state until success. The coherence times of the electron spin associated with the NV center is longer than 10 ms by using dynamical decoupling techniques. A short 2 ns optical resonant transition time and the subnanosecond electron-spin manipulation have been achieved in experiments. Therefore, the timescales of our schemes can be neglected.

### 3 Discussion and summary

Based on parity measurement, in 2004, Beenakker et al. [18] presented a procedure, which requires additional qubit, to realize a CNOT gate acting on two flying electronic qubits, and no method is presented for the  $(\text{SWAP})^a$  gate. According to the optimal synthesis procedure (the optimal cost of a SWAP gate is 3 CNOT or 3 controlled-phase-flip gates), Liang et al. [68] designed a quantum circuit for a SWAP gate acting on a flying and a stationary qubits in 2005. In 2010, Koshino et al. [69] proposed a scheme for implementing a photon-photon  $\sqrt{\text{SWAP}}$  gate assisted with an atomic medium. Zhang et al. [36] proposed a scheme for implementing a robust  $\sqrt{\text{SWAP}}$  gate on diamond NV centers. It is known that one CNOT gate can be realized by combining 2  $\sqrt{\text{SWAP}}$  gates and 3 single-qubit rotations [5]. That is, the optimal cost of a general two-qubit operation is 6  $\sqrt{\text{SWAP}}$  gates. Fan et al. [2] pointed out that 3  $(\text{SWAP})^a$  gates with the help of 6 single-qubit gates are sufficient to realize an arbitrary two-qubit quantum computation.

In conclusion, we have designed the compact quantum circuits for implementing the  $(\text{SWAP})^a$  and SWAP gates on two diamond NV centers coupled to resonators by some input-output processes of a single photon. The cost of a circuit for any two-qubit operation in terms of the  $(\text{SWAP})^a$  gate beats the  $\sqrt{\text{SWAP}}$  gate largely. Our schemes have some features. First, the electronic qubits involved in these gates are the stationary ones, not the flying ones, which reduces the interaction between each electron-spin qubit and its environment. Compared with the gates on atomic qubits, these gates have good scalability. Second, the complexity of our schemes for the  $(\text{SWAP})^a$  and SWAP gates beat their optimal synthesis and beat the ones based on parity-check measurement which requires additional electronic qubits largely. The optimal synthesis of a SWAP or  $\sqrt{\text{SWAP}}$  gate requires 3 CNOT gates. Third, our schemes are economic as additional electronic qubits are not employed. Fourth, the success probability of our scalable schemes is 100 % in principle. Fifth, the fidelities of our schemes with the undegeneracy sublevels  $|+\rangle$  and  $|-\rangle$  are higher than the ones employed the degeneracy sublevels. Moreover, our schemes are feasible in experiment with current technology.

**Acknowledgments** This work is supported by the National Natural Science Foundation of China under Grant No. 11174039 and NECT-11-0031.

## References

1. Nielsen, M.A., Chuang, I.L.: Quantum Computation and Quantum Information. Cambridge University Press, Cambridge (2000)
2. Fan, H., Roychowdhury, V., Szkopek, T.: Optimal two-qubit quantum circuits using exchange interactions. *Phys. Rev. A* **72**, 052323 (2005)
3. Roberto, J.G.: Effect of the Dzyaloshinski-Moriya term in the quantum SWAP <sup>$\alpha$</sup>  gate produced with exchange coupling. *Phys. Rev. A* **77**, 012331 (2008)
4. Balakrishnan, S., Sankaranarayanan, R.: Entangling characterization of SWAP<sup>1/ $m$</sup>  and controlled unitary gates. *Phys. Rev. A* **78**, 052305 (2008)
5. Loss, D., DiVincenzo, D.P.: Quantum computation with quantum dots. *Phys. Rev. A* **57**, 120–126 (1998)
6. Knill, E., Laflamme, R., Milburn, G.J.: A scheme for efficient quantum computation with linear optics. *Nature* **409**, 46–52 (2001)
7. Feng, G.R., Xu, G.F., Long, G.L.: Experimental realization of nonadiabatic holonomic quantum computation. *Phys. Rev. Lett.* **110**, 190501 (2013)
8. Ren, B.C., Wei, H.R., Deng, F.G.: Deterministic photonic spatial-polarization hyper-controlled-not gate assisted by a quantum dot inside a one-side optical microcavity. *Laser Phys. Lett.* **10**, 095202 (2013)
9. Ren, B.C., Deng, F.G.: Hyper-parallel photonic quantum computation with coupled quantum dots. *Sci. Rep.* **4**, 4623 (2014)
10. Duan, L.M., Kimble, H.J.: Scalable photonic quantum computation through cavity-assisted interactions. *Phys. Rev. Lett.* **92**, 127902 (2004)
11. Wei, H.R., Deng, F.G.: Universal quantum gates for hybrid systems assisted by quantum dots inside double-sided optical microcavities. *Phys. Rev. A* **87**, 022305 (2013)
12. Wei, H.R., Deng, F.G.: Scalable photonic quantum computing assisted by quantum-dot spin in double-sided optical microcavity. *Opt. Express* **21**, 17671 (2013)
13. Wei, H.R., Deng, F.G.: Universal quantum gates on electron-spin qubits with quantum dots inside single-side optical microcavities. *Opt. Express* **22**, 593–607 (2014)
14. Xu, G.F., Zhang, J., Tong, D.M., Sjöqvist, E., Kwek, L.C.: Nonadiabatic holonomic quantum computation in decoherence-free subspaces. *Phys. Rev. Lett.* **109**, 170501 (2012)
15. Long, G.L., Xiao, L.: Parallel quantum computing in a single ensemble quantum computer. *Phys. Rev. A* **69**, 052303 (2004)
16. Hua, M., Tao, M.J., Deng, F.G.: Universal quantum gates on microwave photons assisted by circuit quantum electrodynamics. *Phys. Rev. A* **90**, 012328 (2014)
17. Nemoto, K., Munro, W.J.: Nearly deterministic linear optical controlled-not gate. *Phys. Rev. Lett.* **93**, 250502 (2004)
18. Beenakker, C.W.J., DiVincenzo, D.P., Emary, C., Kindermann, M.: Charge detection enables free-electron quantum computation. *Phys. Rev. Lett.* **93**, 020501 (2004)
19. Lin, Q., Li, J.: Quantum control gates with weak cross-Kerr nonlinearity. *Phys. Rev. A* **79**, 022301 (2009)
20. Lin, Q., He, B.: Single-photon logic gates using minimal resources. *Phys. Rev. A* **80**, 042310 (2009)
21. Hu, C.Y., Young, A., O'Brien, J.L., Munro, W.J., Rarity, J.G.: Giant optical Faraday rotation induced by a single-electron spin in a quantum dot: applications to entangling remote spins via a single photon. *Phys. Rev. B* **78**, 085307 (2008)
22. Hu, C.Y., Munro, W.J., Rarity, J.G.: Deterministic photon entangler using a charged quantum dot inside a microcavity. *Phys. Rev. B* **78**, 125318 (2008)
23. Bonato, C., Haupt, F., Oemrawsingh, S.S.R., Gudat, J., Ding, D., van Exter, M.P., Bouwmeester, D.: CNOT and Bell-state analysis in the weak-coupling cavity QED regime. *Phys. Rev. Lett.* **104**, 160503 (2010)
24. Wang, H.F., Zhu, A.D., Zhang, S., Yeon, K.H.: Optically controlled phase gate and teleportation of a controlled-NOT gate for spin qubits in a quantum-dot-microcavity coupled system. *Phys. Rev. A* **87**, 062337 (2013)

25. Wang, H.F., Zhu, A.D., Zhang, S.: One-step implementation of multiqubit phase gate with one control qubit and multiple target qubits in coupled cavities. *Opt. Lett.* **39**, 1489–1492 (2014)
26. Wang, H.F., Zhu, A.D., Zhang, S.: Physical optimization of quantum error correction circuits with spatially separated quantum dot spins. *Opt. Express* **21**, 12484–12494 (2013)
27. Wang, H.F., Zhu, A.D., Zhang, S., Yeon, K.H.: Deterministic CNOT gate and entanglement swapping for photonic qubits using a quantum-dot spin in a double-sided optical microcavity. *Phys. Lett. A* **377**, 2870–2876 (2013)
28. Burkard, G.: A cavity-mediated quantum CPHASE gate between NV spin qubits in diamond. [arXiv:1402.6351v1](https://arxiv.org/abs/1402.6351v1)
29. Balasubramanian, G., Neumann, P., Twitchen, D., Markham, M., Kolesov, R., Mizuochi, N., Isoya, J., Achard, J., Beck, J., Tissler, J., Jacques, V., Hemmer, P.R., Jelezko, F., Wrachtrup, J.: Ultralong spin coherence time in isotopically engineered diamond. *Nat. Mater.* **8**, 383–387 (2009)
30. Jelezko, F., Gaebel, T., Popa, I., Gruber, A., Wrachtrup, J.: Observation of coherent oscillations in a single electron spin. *Phys. Rev. Lett.* **92**, 076401 (2004)
31. Fuchs, G.D., Dobrovitski, V.V., Toyli, D.M., Heremans, F.J., Awschalom, D.D.: Gigahertz dynamics of a strongly driven single quantum spin. *Science* **326**, 1520–1522 (2009)
32. Buckley, B.B., Fuchs, G.D., Bassett, L.C., Awschalom, D.D.: Spin-light coherence for single-spin measurement and control in diamond. *Science* **330**, 1212–1215 (2010)
33. Robledo, L., Childress, L., Bernien, H., Hensen, B., Alkemade, P.F.A., Hanson, R.: High-fidelity projective read-out of a solid-state spin quantum register. *Nature* **477**, 574–578 (2011)
34. Yang, W.L., Yin, Z.Q., Xu, Z.Y., Feng, M., Du, J.F.: One-step implementation of multiqubit conditional phase gating with nitrogen-vacancy centers coupled to a high- $Q$  silica microsphere cavity. *Appl. Phys. Lett.* **96**, 241113 (2010)
35. Wei, H.R., Deng, F.G.: Compact quantum gates on electron-spin qubits assisted by diamond nitrogen-vacancy centers inside cavities. *Phys. Rev. A* **88**, 042323 (2013)
36. Zhang, S., Shao, X.Q., Chen, L., Zhao, Y.F., Yeon, K.H.: Robust  $\sqrt{\text{SWAP}}$  gate on nitrogen-vacancy centres via quantum Zeno dynamics. *J. Phys. B At. Mol. Opt. Phys.* **44**, 075505 (2011)
37. Jelezko, F., Gaebel, T., Popa, I., Domhan, M., Gruber, A., Wrachtrup, J.: Observation of coherent oscillation of a single nuclear spin and realization of a two-qubit conditional quantum gate. *Phys. Rev. Lett.* **93**, 130501 (2004)
38. van der Sar, T., Wang, Z.H., Blok, M.S., Bernien, H., Tamini, T.H., Toyli, D.M., Lidar, D.A., Awschalom, D.D., Hanson, R., Dobrovitski, V.V.: Decoherence-protected quantum gates for a hybrid solid-state spin register. *Nature* **484**, 82–86 (2012)
39. Wang, C., Zhang, Y., Jiao, R.Z., Jin, G.S.: Universal quantum controlled phase gates on photonic qubits based on nitrogen vacancy centers and microcavity resonators. *Opt. Express* **21**, 19252–19260 (2013)
40. Ren, B.C., Deng, F.G.: Hyperentanglement purification and concentration assisted by diamond NV centers inside photonic crystal cavities. *Laser Phys. Lett.* **10**, 115201 (2013)
41. Hu, C.Y., Munro, W.J., O'Brien, J.L., Rarity, J.G.: Proposed entanglement beam splitter using a quantum-dot spin in a double-sided optical microcavity. *Phys. Rev. B* **80**, 205326 (2009)
42. Hu, C.Y., Rarity, J.G.: Loss-resistant state teleportation and entanglement swapping using a quantum-dot spin in an optical microcavity. *Phys. Rev. B* **83**, 115303 (2011)
43. Young, A.B., Oulton, R., Hu, C.Y., Thijssen, A.C.T., Schneider, C., Reitzenstein, S., Kamp, M., Höing, S., Worschech, L., Forchel, A., Rarity, J.G.: Quantum-dot-induced phase shift in a pillar microcavity. *Phys. Rev. A* **84**, 011803(R) (2011)
44. Cheng, L.Y., Wang, H.F., Zhang, S., Yeon, K.H.: Quantum state engineering with nitrogen-vacancy centers coupled to low- $Q$  microresonator. *Opt. Express* **21**, 5988–5997 (2013)
45. Zheng, A.S., Li, J.H., Yu, R., Lu, X.Y., Wu, Y.: Generation of Greenberger-Horne-Zeilinger state of distant diamond nitrogen-vacancy centers via nanocavity input-output process. *Opt. Express* **20**, 16902 (2012)
46. Chen, Q., Feng, M.: Quantum gating on neutral atoms in low- $Q$  cavities by a single-photon input-output process. *Phys. Rev. A* **79**, 064304 (2009)
47. Wang, T.J., Song, S.Y., Long, G.L.: Quantum repeater based on spatial entanglement of photons and quantum-dot spins in optical microcavities. *Phys. Rev. A* **85**, 062311 (2012)
48. Wang, T.J., Lu, Y., Long, G.L.: Generation and complete analysis of the hyperentangled Bell state for photons assisted by quantum-dot spins in optical microcavities. *Phys. Rev. A* **86**, 042337 (2012)
49. Wang, C.: Efficient entanglement concentration for partially entangled electrons using a quantum-dot and microcavity coupled system. *Phys. Rev. A* **86**, 012323 (2012)

50. Wang, C., Zhang, Y., Jin, G.S.: Entanglement purification and concentration of electron-spin entangled states using quantum dot spins in optical microcavities. *Phys. Rev. A* **84**, 032307 (2011)
51. Luxmoore, I.J., Ahmadi, E.D., Luxmoore, B.J., Wasley, N.A., Tartakovskii, A.I., Hugues, M., Skolnick, M.S., Fox, A.M.: Restoring mode degeneracy in H1 photonic crystal cavities by uniaxial strain tuning. *Appl. Phys. Lett.* **100**, 121116 (2012)
52. Bonato, C., Ding, D., Gudat, J., Thon, S., Kim, H., Petroff, P.M., van Exter, M.P., Bouwmeester, D.: Tuning micropillar cavity birefringence by laser induced surface defects. *Appl. Phys. Lett.* **95**, 251104 (2009)
53. Gudat, J., Bonato, C., van Nieuwenburg, E., Thon, S., Kim, H., Petroff, P.M., van Exter, M.P., Bouwmeester, D.: Permanent tuning of quantum dot transitions to degenerate microcavity resonances. *Appl. Phys. Lett.* **98**, 121111 (2011)
54. Bonato, C., van Nieuwenburg, E., Gudat, J., Thon, S., Kim, H., van Exter, M.P., Bouwmeester, D.: Strain tuning of quantum dot optical transitions via laser-induced surface defects. *Phys. Rev. B* **84**, 075306 (2011)
55. Albrecht, R., Bommer, A., Deutsch, C., Reichel, J., Becher, C.: Coupling of a single nitrogen-vacancy center in diamond to a fiber-based microcavity. *Phys. Rev. Lett.* **110**, 243602 (2013)
56. Manson, N.B., Harrison, J.P., Sellars, M.J.: Nitrogen-vacancy center in diamond: model of the electronic structure and associated dynamics. *Phys. Rev. B* **74**, 104303 (2006)
57. Togan, E., Chu, Y., Trifonov, A.S., Jiang, L., Maze, J., Childress, L., Dutt, M.V.G.: Quantum entanglement between an optical photon and a solid-state spin qubit. *Nature* **466**, 730–734 (2010)
58. Walls, D.F., Milburn, G.J.: *Quantum Optics*. Springer, Berlin (1994)
59. An, J.H., Feng, M., Oh, C.H.: Quantum-information processing with a single photon by an input-output process with respect to low- $Q$  cavities. *Phys. Rev. A* **79**, 032303 (2009)
60. Chen, Q., Yang, W.L., Feng, M., Du, J.F.: Entangling separate nitrogen-vacancy centers in a scalable fashion via coupling to microtoroidal resonators. *Phys. Rev. A* **83**, 054305 (2011)
61. Shende, V.V., Bullock, S.S., Markov, I.L.: Recognizing small-circuit structure in two-qubit operations. *Phys. Rev. A* **70**, 012310 (2004)
62. Vatan, F., Williams, C.: Optimal quantum circuits for general two-qubit gates. *Phys. Rev. A* **69**, 032315 (2004)
63. Zhang, Y.S., Ye, M.Y., Guo, G.C.: Conditions for optimal construction of two-qubit nonlocal gates. *Phys. Rev. A* **71**, 062331 (2005)
64. Barclay, P.E., Fu, K.M.C., Santori, C., Beausoleil, R.G.: Chip-based microcavities coupled to nitrogen-vacancy centers in single crystal diamond. *Appl. Phys. Lett.* **95**, 191115 (2009)
65. Larsson, M., Dinyari, K.N., Wang, H.: Composite optical microcavity of diamond nanopillar and silica microsphere. *Nano Lett.* **9**, 1447–1450 (2009)
66. Barclay, P.E., Fu, K.M., Santori, C., Beausoleil, R.G.: Hybrid photonic crystal cavity and waveguide for coupling to diamond NV-centers. *Opt. Express* **17**, 9588–9601 (2009)
67. Bernien, H., Hensen, B., Pfaff, W., Koolstra, G., Blok, M.S., Robledo, L., Tamniak, T.H., Markham, M., Twitchen, D.J., Childress, L., Hanson, R.: Heralded entanglement between solid-state qubits separated by three metres. *Nature* **497**, 86 (2013)
68. Liang, L.M., Li, C.Z.: Realization of quantum SWAP gate between flying and stationary qubits. *Phys. Rev. A* **72**, 024303 (2005)
69. Koshino, K., Ishizaka, S., Nakamura, Y.: Deterministic photon-photon  $\sqrt{\text{SWAP}}$  gate using a  $\Lambda$  system. *Phys. Rev. A* **82**, 010301 (2010)